WATER RESOURCES RESEARCH, VOL. 21, NO. 8, PAGES 1233–1250, AUGUST 1985

Generalized Scale Invariance in the Atmosphere and Fractal Models of Rain

S. LOVEJOY[1] AND D. SCHERTZER[2]

Etablissement d'Etudes et Recherches Météorologiques/Centre de Recherches en Météorologie Dynamique Météorologie Nationale, Paris

In recent years there has been considerable interest in stochastic rain models. By developing new ideas about scale invariance and intermittency we argue that the scope of such models can be greatly extended. The notions of scale invariance, intermittency, and the associated idea of fractal dimension have lately gained considerable ground, particularly in the context of extremely variable phenomena such as those found in the mesoscale and in hydrodynamic turbulence. We review some relevant work and argue that the atmosphere respects a symmetry principle that we call generalized scale invariance in which the statistical properties of the small and large scale are related to each other by a magnification coupled with a differential stratification (due to gravity) and differential rotation (due to the Coriolis force). We further argue that the extremely erratic (intermittent) nature of the atmosphere is characterized by scale invariant (fractal) measures leading to hyperbolic (fat-tailed) probability distributions of the fluctuations. The standard statistical methods based on exponential fall offs in both correlations and probability distributions are inappropriate when the variability is of this type. We show how both the scaling and intermittency may be exploited to develop extremely variable stochastic models of rain. Although the models examined here are the simplest of a family of extremely variable processes (depending on only two radar-determined parameters), they lead to realizations possessing many realistic features of the rainfield including complexity of form, clustering and bands at all scales, as well as differential stratification and rotation. Finally, we point to weaknesses in the models (in particular, their monodimensional nature) and suggest possible improvements.

1. INTRODUCTION

One of the great successes of physics in the last decade has been in the understanding of phenomena with fluctuations over many scales. In high-energy physics, critical phenomena, and hydrodynamics it is often possible to establish the existence of a scaling or scale invariant regime in which the fluctuations (ΔX) in the field of interest (X) at small scale Δt and at large scale $\lambda\Delta t$ ($\lambda > 1$) are amplified by the factor λ^H, where H is the scaling parameter. This may be written more concisely as

$$\Delta X(\lambda\Delta t) = {}^{d}\lambda^{H}\Delta X(\Delta t)$$

where $\Delta t = t_1 - t_0$, $\Delta X(\Delta t) = X(t_1) - X(t_0)$, $t_2 = t_0 + \lambda(t_1 - t_0)$, $\Delta X(\lambda\Delta t) = X(t_2) - X(t_0)$, and equality is understood in the sense of probability distributions (that is, $X \stackrel{d}{=} Y$ if $Pr(X > q) = Pr(Y > q)$ for all q, Pr means "probability").

The amplification, or renormalization, of the fluctuations can be understood as a double zoom (both of physical space and the field) which leaves the phenomena invariant, hence the notion of scale invariance.

The principle arguments and evidence for scale invariance in the atmosphere may be found in the works by *Lovejoy* [1981, 1982, 1983] and *Lovejoy and Schertzer* [1985a; *Schertzer and Lovejoy*, 1984*a*, *b*, 1985a, *b*, also unpublished manuscript, 1983] [see also *Hentschel and Procaccia*, 1984 and *Waymire*, 1985]. In summary, they are, first, the relevant equations are almost certainly scale invariant. For example, the basic equations of the atmosphere, those of Navier-Stokes, involve no characteristic lengths above a small viscous scale, which in the atmosphere is of the order of millimeters. Hence the equations admit scaling solutions. Second, the boundary conditions such as topography and solar forcing also appear to be scale invariant [see *Schertzer and Lovejoy*, 1985a]. Other arguments for scale invariance can be found: *Waymire* [1985] argues that if the rain field is regarded as being the sum of a large number of randomly distributed elementary pulses, scaling should result, since, in general, such sums tend to scaling limits. Empirically, a considerable body of evidence, mostly from the mesoscale (c.f. the excellent review by *Lilly* [1983]), shows (1) out to at least 1000 km, the energy spectrum of the horizontal wind in the horizontal is of the scaling form $k^{-\beta_h}$ (k is a wave number) and $\beta_h \sim 5/3$ (i.e., there is apparently no mesoscale spectral gap) and (2) the corresponding spectrum in the vertical is of the same form but with a very different exponent (β_v) of value roughly $\frac{11}{5}$. These whole number fractions are used because they may be derived using dimensional arguments: the (Kolmogorov) $\frac{5}{3}$ value by assuming energy transfer to dominate in the horizontal and $\frac{11}{5}$; see, for example, *Bogliano* [1959], *Obukhov* [1959], and *Schertzer and Lovejoy* [1985]) by assuming buoyancy force variance flux to dominate in the vertical. The other exponents used in this paper are also given in similar fractional form because eventually, similar kinds of arguments might enable them to be derived theoretically. It is worth noting that for finite variance, the spectral exponent β is simply related to the scaling exponent H by the formula $\beta = 2H + 1$ which follows from the fact that the moment of order 2 (the variance) of the fluctuations can be expressed as an integral of the energy spectrum.

Although the atmosphere exhibits fluctuations over scales differing by a factor of a billion or so (10^6 to 10^{-3}m), it is manifestly not isotropic: gravity leads to stratification, and

[1] Now at Physics Department, McGill University, Montreal, Quebec.

[2] Now at Physics Department, McGill University, Montreal, Quebec.

Paper number 5W0289.
0043-1397/85/005W-0289$05.00

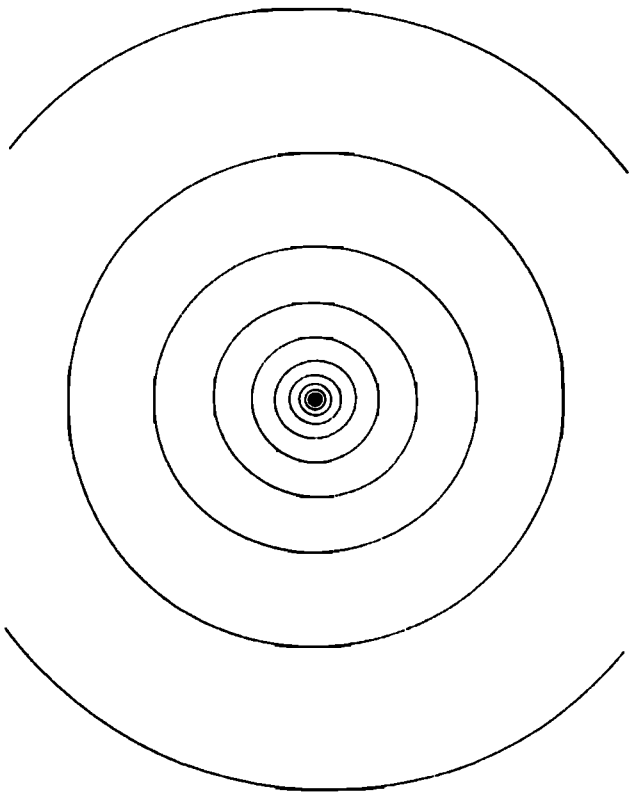

Fig. 1*a*. Family of two-dimensional balls in an isotropic metric (circles), indicating distances from the center increasing by factors of 1.28. The distance between two points is defined by the radius of the ball centered on one of the points and intersecting the other. The area of the balls increases as λ^2 as the size (λ) increases, hence the dimension =2.

the Coriolis force leads to rotation. In general, the possibility of scale invariance has only been considered in isotropic systems, in which case the small scale is an exact copy of the large; hence the fluctuations are self-similar. The atmosphere cannot be self-similar; if it was, then we would expect to find clouds thousands of kilometers thick! Ever since *Richardson* [1922], the basic phenomenology of turbulence has consisted of an isotropic cascade of energy from large to small scales (for contemporary reviews see *Orszag* [1973] or *Rose and Sulem* [1978]). *Schertzer and Lovejoy* [1983, 1985*a*] considered anisotropic cascades in order to account for differential vertical stratification. This natural idea leads to the surprising conclusion that the effective dimension (called an elliptical dimension, D_{el}) of the atmosphere is $\frac{23}{9}$ = 2.5555... rather than 2 or 3 as in the usual models. Figures 1*a* and 1*b* compare the shape of the average eddies in the isotropic and anisotropic cases. The new dimension D_{el} is called an elliptical dimension because of these ellipsoids. However, the atmosphere exhibits not only differential stratification, but also differential rotation which lead *Schertzer and Lovejoy* [1985*b*] to propose a more general notion of scale invariance ("generalized scale invariance" (GSI)) which involves modifying the metric.

At the very least, a scale invariant model of the atmosphere must include the effects of differential rotation and stratification. This, however, is insufficient: the atmosphere is also known to be extremely intermittent (erratic) and to be characterized by a rich diversity of structures. One early attempt to account for intermittency was *Kolmogorov*'s [1962] proposal that the energy flux was lognormally distributed (i.e., that the probability distribution was long tailed, but not truely fattailed (hyperbolic)). Attempts to theoretically model intermittency lead, via the work of *Novikov and Stewart* [1964] and *Yaglom* [1966], to *Mandelbrot*'s [1974] very general cascade scheme. In such a cascade, Mandelbrot showed the transfer of energy flux was generally hyperbolically distributed. He also pointed out that lognormality involves several internal (theoretical) contradictions. *Schertzer and Lovejoy* [1983, 1985*a*] proposed that such "hyperbolic intermittency" is a general feature of atmospheric fluctuations. This means that the probability of a random fluctuation $\Delta X'$ exceeding a fixed ΔX is of the form

$$Pr(\Delta X' > \Delta X) \propto \Delta X^{-\alpha}$$

for large ΔX; α is the hyperbolic exponent associated with

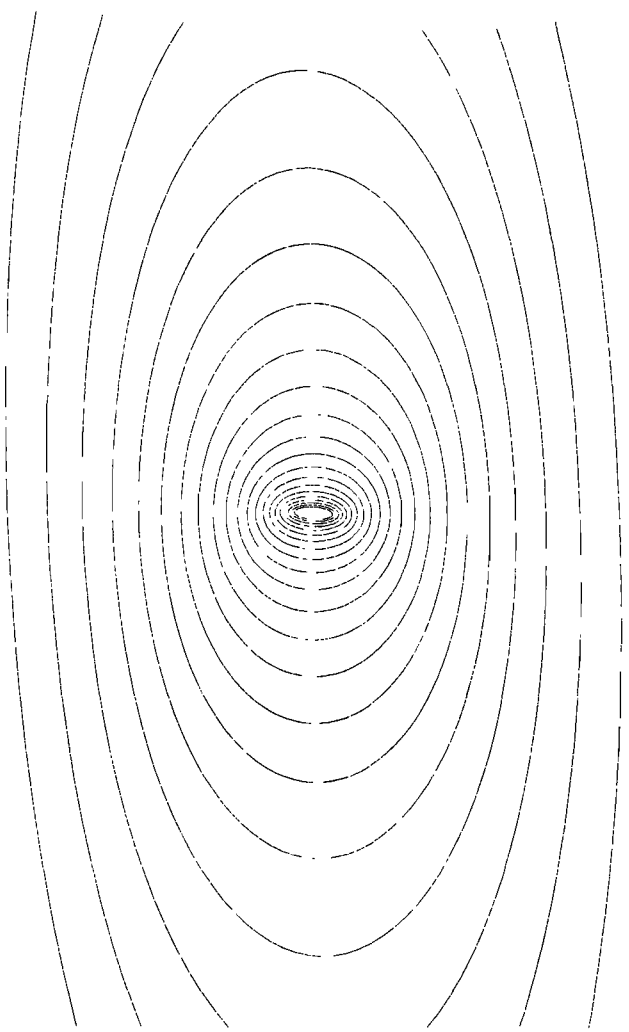

Fig. 1*b*. Same family of balls in the anisotropic case (corresponding to $\mathbf{G} = \begin{pmatrix} 1 & 0 \\ 0 & 5/9 \end{pmatrix}$; see section 3). The shape of the balls model the average eddy shape; the flattening of the large balls models the fact that the atmosphere is increasingly stratified at large scale, and the small-scale vertically oriented balls corresponds to "convective" type eddies. The area of the balls increases as $\lambda\lambda^{5/9} = \lambda^{1.5555}$ (the product of the major and minor axes) as the size of the balls increases, thus the effective dimension is 1.5555 . . . rather than 2.

intermittency. Note that the smaller α, the more extreme the fluctuations. Furthermore, high-order moments $\langle \Delta X^h \rangle$ with $h \geq \alpha$ diverge (of course, empirical moments which are averages of empirical values are always finite: the divergence of moments simply means that the latter increase without limit as the sample size increases). Empirically, $\alpha = \frac{5}{3}$ for the rainfield [*Lovejoy*, 1981], $\frac{5}{3}$, $\frac{10}{3}$, 1, 5 for the rate of energy transfer, buoyancy, force variance, Richardson number, and the velocity field, respectively [*Schertzer and Lovejoy*, 1985*a*, also unpublished manuscript, 1983], 5 for temperature fluctuations [*Lovejoy and Schertzer*, 1985*a*, *b*] 1 for radar reflectivity [*Lovejoy and Schertzer*, 1985*c*], and 2 for rain and cloud drop volumes (S. Lovejoy and D. Schertzer unpublished data, 1985).

Another basic feature of the fluctuations in Mandelbrot's model is that the increasingly active (intense) regions of such a field are concentrated in sets of decreasing fractal dimension [*Mandelbrot*, 1984; D. Schertzer and S. Lovejoy, unpublished manuscript, 1983]. In other words, for a field X, on average, the number of regions at scale L exceeding a given intensity threshold (T) is $\propto L^{D(T)}$ with $D(T) < E$ (E is the euclidean dimension of space), and $D(T)$ is a decreasing function of T.

Lovejoy and Mandlebrot [1985] proposed a simple model of rain based on the fractal sums of pulses (FSP) process (B. Mandelbrot, unpublished manuscript, 1985) which is both scaling and hyperbolically intermittent [see also Waymire, this issue]. Although this model produced cloud and rain fields that were fairly realistic visually and statistically, they suffered from at least four limitations: (1) they are self-similar (isotropic); (2) the scaling parameter H cannot be varied independently of the intermittency parameter ($\alpha = \frac{1}{H}$); (3) the physical interpretation is artificial; and (4) the intermittency of the rainfield it generates is characterized by a single fractal dimension. The object of the following paper is to attempt to overcome these limitations and thereby produce more realistic cloud and rain simulations. It should be clear that these models are merely the simplest of a family of extremely variable anisotropic models with fluctuations over a wide range of space and time scales. Indeed, given the simplicity of these models, their visually realistic character is quite surprising (the reader is encouraged to survey the figures before continuing). Models of this type are probably indispensible in modeling in hydrology, meteorology, remote sensing, and statistics.

This paper is structured as follows: first there is a summary of previous work, in particular, a résumé of the simplest fractal models (section 2), and there is a summary of the formalism of generalized scale invariance (section 3). The two are then combined, yielding simulations of vertical rain and cloud cross sections and of the effect of the Coriolis force, including comparisons with satellite photographs (section 4). In section 5 the FSP process is generalized somewhat to the scaling cluster of pulses (SCP) process so as to allow H, α to be independently varied and to yield a more physically appealing process. The SCP process allows crude simulations of the cloud field associated with mid-latitude cyclones. In section 6 an efficient numerical algorithm is described which, by iterative "zooming" (numerical renormalization), enables the fractal dimensions of these processes to be calculated with high accuracy. In section 7 we examine the issue of intermittency and multidimensionality. Section 8 is devoted to conclusions.

2. Fractal Sums of Pulses Process

2.1. Empirical Evidence

The FSP process is described in the work by B. Mandelbrot (unpublished manuscript, 1985). It has two basic features: (1) hyperbolically distributed fluctuations and (2) scale invariance. *Lovejoy and Mandelbrot* [1985] summarize and augment the empirical evidence in favor of using such models for the rain field and describe and illustrate the implementation of this process in one, two, and three dimensions (time series and horizontal rain cross sections and their temporal evolution). The physical relevance of the various model assumptions will be discussed in section 5.

The empirical evidence comes from radar and satellite data analyzed in the works by *Lovejoy* [1981, 1982, 1983] and *Lovejoy et al.* [1983]. Horizontal scaling was established by using the area (A)-perimeter (P) relationship [*Mandelbrot*, 1977] which relates fractal areas to perimeters by the formula $P \propto (\sqrt{A})^{D_p}$, where D_p is the dimension of the perimeter. Smooth perimeters satisfy $P \propto A$, hence $D_p \sim 1$ and maximally complicated perimeters that literally fill the plane satisfy $P \propto A$, hence $D_p \sim 2$. *Lovejoy* [1982] found $D_p \sim 1.35$ for rain and cloud areas between 1 km^2 and 1.2×10^6 km^2, the lower limit being recently extended by R. Cahalan et al. (unpublished manuscript, 1984) to 2.6×10^{-2} km^2 with Landsat imagery. The scaling of perimeters over the range of length scales 0.16 to 1000 km is direct support for the horizontal scaling of the rain and cloud fields. Note that approximately the same value of D_p was obtained over the Indian Ocean, Tropical Atlantic, France, and the Mediterannean.

The horizontal scaling exponent H was determined from radar data in two ways. First, it was determined directly from the probability distributions of rainfall gradients over different distances of separation (Δx) which yielded $H \sim 0.50$ (specifically, it was shown that $\Delta R(\lambda \Delta x) \propto \lambda^{0.50} \Delta R(\Delta x)$ for various values of $\lambda \Delta x$, and Δx). A precise determination ($H = 0.48 \pm 0.02$) was obtained using a robust measure of dependency called R/S analysis (*Mandelbrot* [1972]; for some of the difficulties involved with this method, which include a bias for short series, see *Bhattacharya et al.* [1983], and for another geophysical example of its application see *Lovejoy and Schertzer* [1985*b*]).

Temporal scaling (at least from 5–40 min) and hyperbolic intermittency were established by examining time histories of total rain flux from isolated storms in Montreal, Spain, and the tropical Atlantic; these were found to be characterized by the following probability distributions: $Pr(\Delta R > \Delta r) \propto \Delta r^{-\alpha}$ for large Δr, the value of α being estimated as 1.66 ± 0.05 in these three locations [*Lovejoy*, 1981; *Lovejoy and Mandelbrot*, 1985]. Note that distributions of this form with $\alpha < 2$ occasionally yield such large values that the largest of a sample of random Δr is of the same order of magnitude as the sum of all the others in the sample. *Mandelbrot and Wallis* [1968] describe this as the "Noah" effect after the extreme fluctuation responsible for the Biblical flood.

Other related evidence for scaling behavior comes from probability distributions of both rain areas and of straight line sections ["fronts"; *Lovejoy et al.*, 1983]. In both cases, we expect to find hyperbolic distributions because any other kind of distribution would involve a length scale and hence break the scaling. Radar data analyzed from the GATE experiment (tropical Atlantic) showed $Pr(A > a) \propto a^{-B}$ with B ~ 0.75 [*Lovejoy*, 1981; *Lovejoy and Mandelbrot*, 1985]. The

probability distribution of straight-line sections of perimeters was also analyzed to determine whether an objective distinction could be made between smooth, rounded rain and cloud perimeters, and long straight frontlike perimeters. An objective method of performing such an analysis called "straight-line sampling" is described in the work by *Lovejoy et al.* [1983]. When the distribution of straight-line lengths (L) was measured by radar and satellite infrared imagery over France, the distribution $Pr(L' > L) \propto L^{-w}$ with $w \sim 3.6$ was obtained showing that any distinction between long linelike perimeter sections ("fronts") and short rounded sections is arbitrary; the distribution of L is not bimodal but falls off gradually in a scale invariant manner.

In summary, the basic scaling and intermittency parameters are $D_p \sim 1.35$, $H \sim 0.50$, and $\alpha \sim 1.66$, with the secondary parameters $B \sim 0.75$ and $w \sim 3.6$. Note that the secondary parameters are mainly of interest in calibrating the models. Unfortunately, they are not generally related to the basic parameters in a simple way (see section 6).

2.2. *Description of the FSP Process*

Consider a function $R(t)$ formed as the sum an infinity of rectangular pulses of random heights representing a rainfall intensity increment ΔR, random widths representing the rainfall duration ρ, and random centers distributed uniformly along the t axis (by a Poisson process with rate ν). If $Pr(\rho' > \rho) \propto \rho^{-1}$ and $\Delta R = \pm \rho^{1/\alpha}$, then the resulting process is scaling parameter $H = 1/\alpha$ because increasing length scales by the factor λ only changes the intensity by the factor $\lambda^{1/\alpha}$. Note that this implies $\langle \rho \rangle \rightarrow \infty$, which is quite different from the usual strongly scale-dependent processes obtained when $Pr(\rho' > \rho)$ is an exponential or other scale-dependent function (see, for example, *Rodriguez-Iturbe et al.* [1984] or *Waymire and Gupta* [1981*a*, *b*, *c*]). The scaling may be understood by the fact that the number of pulses over an interval length L, whose length exceeds ρ is $LPr(\rho' > \rho) = L\rho^{-1}$, which is invariant under the scale transformation $L \rightarrow \lambda L$, $\rho \rightarrow \lambda \rho$. By construction, the increments of the process are hyperbolic with exponent α. B. Mandelbrot (unpublished manuscript, 1985) studies this as well as other FSP processes obtained by modifying the relationship between ρ and ΔR.

To produce rainfield simulations in two dimensions (x, y) the rectangular pulses are first replaced by upright cylinders with circular bases (area A), with height (ΔR) related to A by $\Delta R = \pm A^{1/\alpha}$ and with A chosen so that $Pr(A > a) \propto a^{-1}$. Second, the circular bases of the cylinders are replaced by equal area annuli, such that the unit annulus (area = π) has an outer radius Λ (hence inner radius = $\Lambda^* = (\Lambda^2 - 1)^{1/2}$), and third, the sharp pulse edges are replaced by a smoother function. The final pulse shape used for pulse size ρ(ρ = radius here) was $\Delta R \exp(-((u^2/\rho'^2) - \delta^2)/\sigma^2)^{2s}$; u is the distance from the pulse center; $\Delta R = \pm \rho^{1/\alpha}$ the amplitude; δ is the annulus center ($= \frac{1}{2}(\Lambda^* + \Lambda)$; σ is the width ($= \frac{1}{2}(\Lambda^* - \Lambda)$); and s is a parameter that was introduced to vary the pulse smoothness ($s \rightarrow \infty$ yields sharp-edged rectangular pulses). In practice, we generally took $s = 2$. Furthermore, only pulses between some outer and inner cutoff (ρ_0 and ρ_i, respectively) were used. In the simulations shown here, ρ_0 was taken to be equal to 3 times the size of the simulation "window," and ρ_i was taken to be 1 pixel. We also take $\nu = 1$.

The parameter Λ was introduced to allow for varying degrees of "lacunarity" [*Mandelbrot*, 1982]. Although this concept needs mathematical development, the basic idea is straightforward. As the term suggests, a highly lacunar fractal is characterized by large lacunar (empty) regions. When $\Lambda = 1$, the cylinders have circular bases, and simulated rain fields are dominated by one or two large rain areas with large rain-free zones. When Λ is increased, the lacunarity decreases; i.e., the larger areas break up into clusters of smaller ones and rain areas appear in what were previously rain-free zones. Rainbands also apear; they are produced by the nearly straight sections of enormous annuli. A value of $\Lambda = 1.2$ was found to be visually the most realistic. Note that the importance of clustering phenomena in rainfall is widely recognized and is an essential feature of stochastic rain models [see *Waymire et al.* 1984]. Here the clustering is produced intrinsically by the model. We see later that it seems desirable to enhance the clustering somewhat (section 5).

Figure 2 shows an example of the implementation of this process on an 800 × 800 grid. Note that the field $R(x, y)$ cannot be immediately interpreted in terms of rain rate because the value of $R(x, y)$ is almost surely negative at some points. In practice, a threshold R_T is set, and the rain rate is measured as the difference $R - R_T$, and the remaining negative values are reset to zero (here shown as a black background). The logarithm of the resulting rainfall intensity is then shown on a grey scale with white being the most intense.

If we implement the FSP process in three dimensions (x, y, t) by replacing the annuli by spherical shells (see *Lovejoy and Mandelbrot* [1985] for details), we obtain a model for the temporal evolution. This method of generating temporal evolution is justified by Taylor's hypothesis of "frozen turbulence" which states that temporal statistics are the same as spatial statistics when the latter are dimensionalized by an appropriate velocity factor. *Brown and Robinson* [1979] find Taylor's hypothesis valid up to at least 1000 km distances (for wind spectra; see, however, *Zawadzki* [1973] and *Waymire et al.* [1984] for a discussion of the possibility that the limits of its validity are considerably lower in the rain field). In any case, the comparison between the model and reality will be illuminating. Figures 3*a*–3*c* show an example of the temporal evolution (here black on white background to simulate a radar scope). Note that realistic features of the series are (1) the largest structures "live" longest, (2) they are the most intense, and (3) structures occasionally appear and disappear in a abrupt (intermittent) manner.

For a detailed discussion of the statistical properties of these processes, as well as a large number of samples of the process in both two and a generalization to three dimensions, readers are urged to consult the work by *Lovejoy and Mandelbrot* [1985].

3. GENERALIZED SCALE INVARIANCE

Before discussing anisotropic generalizations of FSP processes it is necessary to explain the formalism of generalized scale invariance as developed in the work by *Schertzer and Lovejoy* [1985*b*].

Consider the operator T_λ that increases scales by a factor λ. We are interested in those T_λ which leave invariant certain basic physical quantities such as energy flux. Obvi-

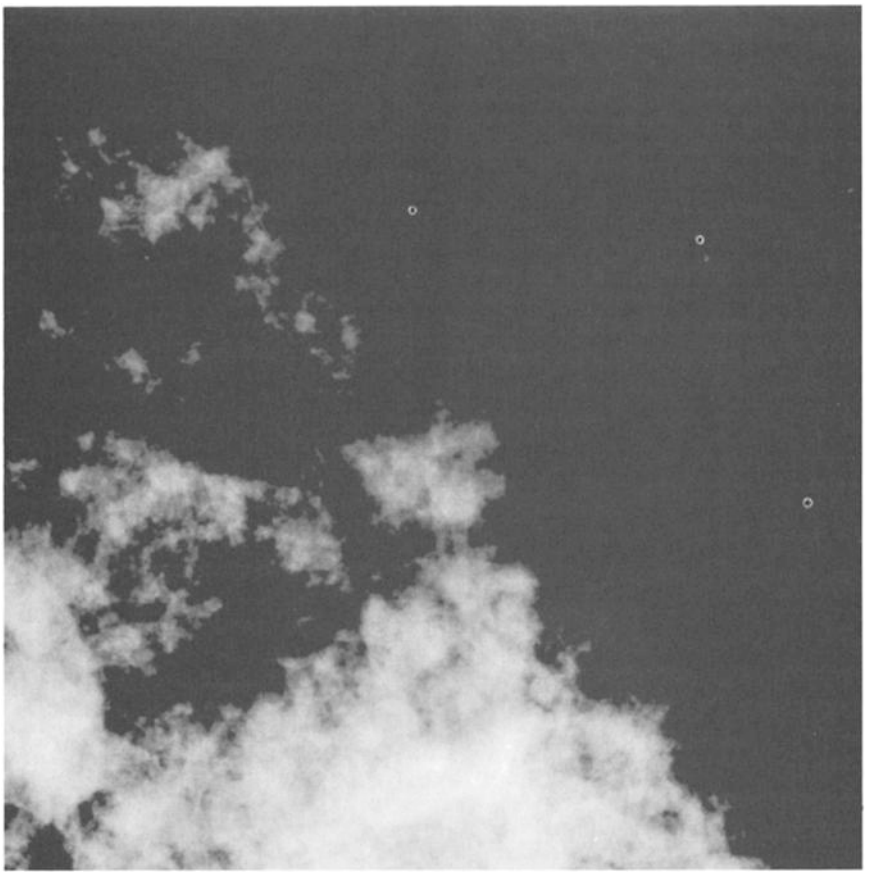

Fig. 2. Example of an isotropic FSP process on an 800 × 800 point grid. The threshold R_T was set so that 70% of the area is rain free (shown in black), and the logarithm of the rain rate is proportional to the whiteness. Here, $\Lambda = 1.2$, $\alpha = \frac{5}{3}$. Note the fairly straight "front" going diagonally from the upper left to lower right-hand corner, which was generated by the edge of an enormous annulus.

ously, the T_λ must satisfy certain properties. They form a group:

$$\forall \lambda \in R^+, \ \mathbf{T}_\lambda \mathbf{T}_{\lambda'} = \mathbf{T}_{\lambda\lambda'}$$

They define balls B_λ increasing with λ such that $B_\lambda = \mathbf{T}_\lambda(B_1)$ with a corresponding metric r:

$$\forall \mathbf{x} \in B_\lambda, \ r(\mathbf{x}) < \lambda$$

In the case of isotropic scaling, $\mathbf{T}_\lambda$ reduces to $\lambda \mathbf{1}$ (a pure dilation).

Schertzer and Lovejoy [1985*b*] were able to obtain an exact result: if **G** is an operator (called the generator of the group) and $\mathbf{T}_\lambda = \exp(\mathbf{G} \log \lambda) = \lambda^{\mathbf{G}}$, then, a necessary and sufficient condition that $\mathbf{T}_\lambda$ is a (linear) generalized scaling operator, is that all the eigenvalues of the linear transformation **G** (i.e., **G** is a matrix) have strictly positive real parts (if, in addition, we require the balls to define a true metric, then the real parts must be strictly greater than 1; see D. Schertzer and S. Lovejoy for the full discussion). If, in order to simplify the discussion we restrict B_1 to be a sphere, then the above conditions apply to the symmetric part of **G**. Note that nonlinear transformations are also possible (these are necessary when the anisotropy is position dependent). Recall that physically we expect the metric to be modified, because in a cascade process, the most natural metric to use is the one in which the balls it defines coincide with the average eddies. In the isotropic case, the balls are self-similar spheres, but when there is a privileged direction we expect these to be replaced by ellipsoids or other convex shapes (the balls B_λ).

In GSI, conserved quantities are measures (μ) (which are not necessarily probability measures) which are invariant under $\mathbf{T}_\lambda$. The simplest case satisfies the following invariance equation:

$$\forall \lambda \in R^+, \ \mu = \lambda^{-D} \mu \mathbf{T}_\lambda$$

with $D \epsilon R^+$ being the dimension of the support of μ. In the case of the usual volume (Lebesgue) measure of the space, D is the elliptical dimension introduced in the works by *Schertzer and Lovejoy* [1985*a*, *b*]:

$$D_{el} = \text{Trace } \mathbf{G} = \log \det (\mathbf{T}_\lambda)$$

The invariance equation involves a single fractal dimension D and therefore in this case, μ is a monodimensional measure. In order to deal with multidimensional measures such as those involved in Mandelbrot's cascade model, a more general invariance equation is necessary. Although further formal discussion of this point is outside the scope of this paper, the relevant phenomenonology is discussed in section 7. In the atmosphere experimental and theoretical results for the dynamical (wind) field suggest $D_{el} = 2 + \frac{5}{9} = \frac{23}{9} = 2.5555 \ldots$, the $\frac{5}{9}$ being the ratio of the horizontal scaling exponent $H_h = \frac{1}{3}$ (which, recalling that $\beta = 2H + 1$, corresponds to the usual Kolmogorov $k^{-5/3}$ spectrum) and

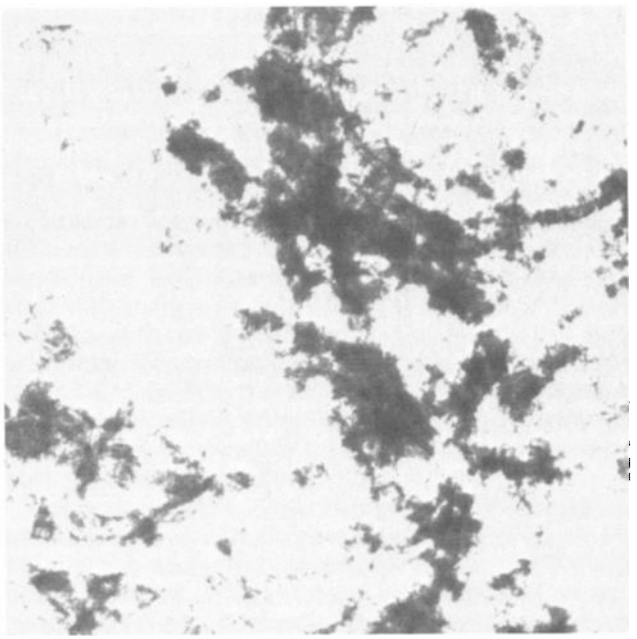

Fig. 3*a*. First of a time series of the FSP process obtained as an x, y section of the three-dimensional (x, y, t) process. The log rain rate is shown on a grey scale on white background on a 400 × 400 grid; $\alpha = \frac{5}{3}$, $\Lambda = 1.2$. Here, $t = 0$.

the vertical exponent $H_v = \frac{3}{5}$ (corresponding to a $k^{-11/5}$ spectrum). Figure 1, which illustrates a vertical cross section with $D_{el} = 1 + \frac{5}{9} = 1.555\ldots$, was obtained by transforming a unit circle by the operator $\mathbf{T}_\lambda = \lambda^{\mathbf{G}}$ with $\mathbf{G} = \begin{pmatrix} 1 & 0 \\ 0 & 5/9 \end{pmatrix}$ for various values of λ. For $\lambda > 1$, the ellipses "flatten" horizontally, eventually resembling "Hadley" type cells; for $\lambda < 1$, they flatten vertically, resembling "convective" type cells. Note that the ellipses represent the shape of average cells. As D_{el} is decreased from 3 to 2, the metric changes from an isotropic three-dimensional metric, through greater and greater degrees of stratification, to an isotropic two-dimensional one.

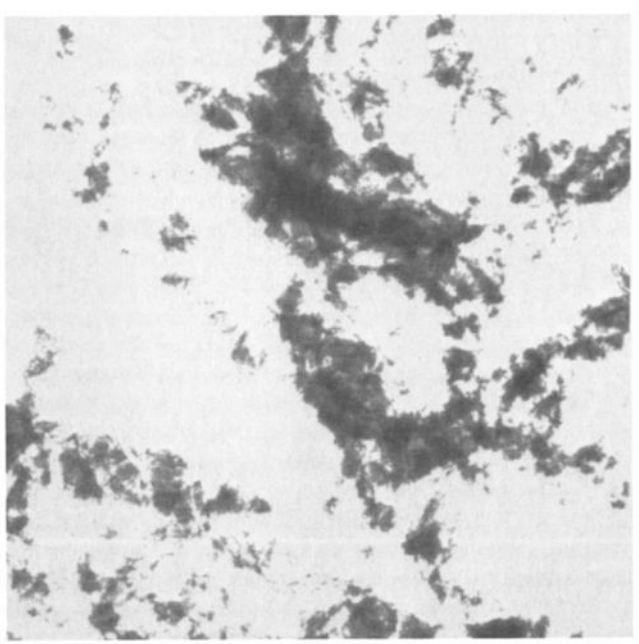

Fig. 3*b*. Same as Figure 3*a* except for $t = 25$ pixels.

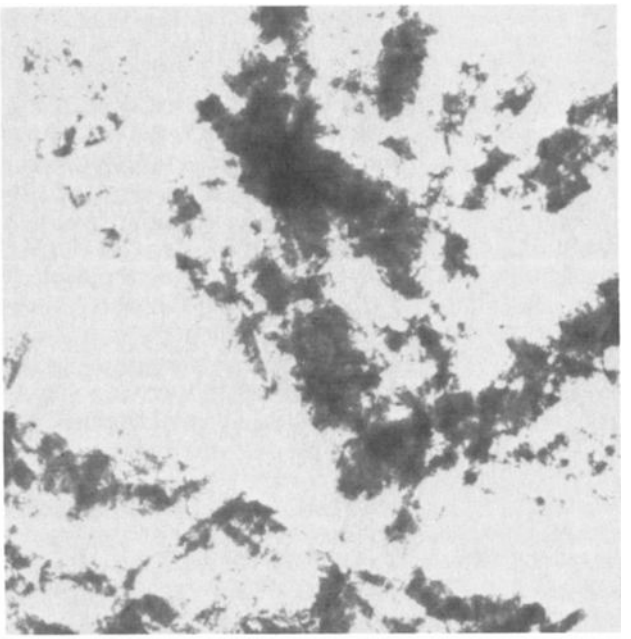

Fig. 3*c*. Same as Figure 3*a* except for $t = 50$ pixels.

In order to effect differential rotation, off-diagonal elements are necessary. In this case, the effect of the operator $\mathbf{T}_\lambda = \lambda^{\mathbf{G}}$ is best understood (and most easily calculated) by decomposing **G** into elementary matrices. In two dimensions this can be easily achieved either by a matrix representation of quaternions [see *Schertzer and Lovejoy*, 1985*b*].

Take

$$\mathbf{1} = \begin{pmatrix} 1 & 0 \\ 0 & 1 \end{pmatrix} \quad \mathbf{I} = \begin{pmatrix} 0 & -1 \\ 1 & 0 \end{pmatrix} \quad \mathbf{J} = \begin{pmatrix} 0 & 1 \\ 1 & 0 \end{pmatrix} \quad \mathbf{K} = \begin{pmatrix} 1 & 0 \\ 0 & -1 \end{pmatrix}$$

note $\mathbf{IJ} = -\mathbf{JI} = -\mathbf{K}$, $\mathbf{JK} = -\mathbf{KJ} = \mathbf{I}$, $\mathbf{KI} = -\mathbf{IK} = -\mathbf{J}$, and $\mathbf{1} = -\mathbf{I}^2 = \mathbf{J}^2 = \mathbf{K}^2$.

G can then be written as a linear combination of the **1**, **I**, **J**, **K**:

$$\mathbf{G} = d\mathbf{1} + c\mathbf{K} + e\mathbf{I} + f\mathbf{J}$$

writing $a^2 = c^2 + f^2 - e^2$ and $u = \log \lambda$, then

$$T_\lambda = \lambda^{\mathbf{G}} = \lambda^d(\mathbf{1} \cosh(au) + (\mathbf{G} - d\mathbf{1}) \sinh(au)/a)$$

The effect of **I** is to rotate, while that of **J**, **K** is to stratify, the values of d, c, e, f determining which effect is predominant; Figures 1*a*, 1*b*, 4*a*, and 4*b* are examples. When the stratification effect dominates ($a^2 > 0$), the axes of the ellipsoids rotate only by $2 \tan^{-1} e/a$ as λ goes from $0 \to \infty$. Note that at $\lambda = 1$, the major axis becomes the minor axis, and visa versa. The apparent rotation is thus $\pi/2$ greater (therefore yielding a total rotation of $\pi/2 + \tan^{-1} e/a$).

This maximum rotation property leads to a prediction about the horizontal structure of rain of cloud fields: when stratification and rotation nearly balance ($a \sim 0$, or when it is negligible: $e \sim 0$), the largest scale structures will be oriented perpendicularly to the smallest scale structures. Figure 5 shows an example of this effect in satellite cloud pictures. When the scale of the transition between large and small (corresponding to $\lambda = 1$, the circles in Figures 1 and 4) are small enough to be perceived by the naked eye, the phenom-

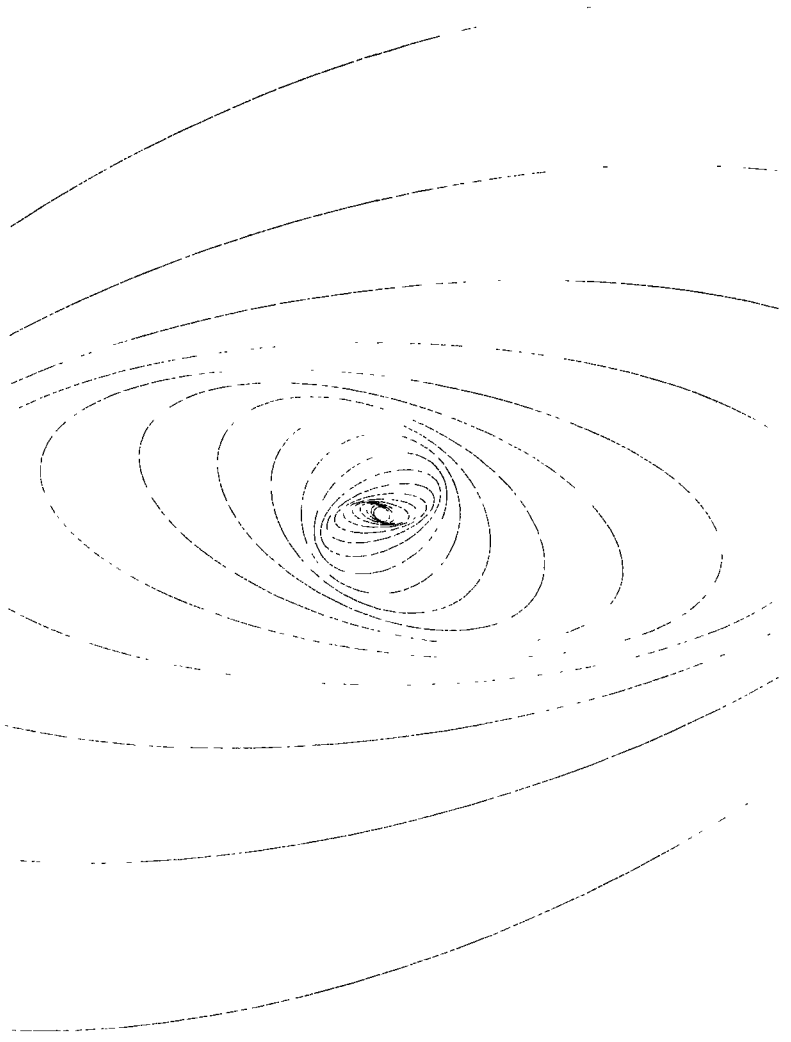

Fig. 4*a*. Same as Figure 1 except for $\mathbf{G}$ ($_{2}^{1}{}_{6}$ $_{1}^{1}{}_{4}$), rotation dominates ($a^2 = -3.64$). Since D_{el} = trace G, here =2 (equals the apparent dimension of the horizontal cross sections of the atmosphere); the balls of the metric could be regarded as defining the anisotropy due to the Coriolis force.

enon may, for example, be responsible for the appearance of "cirrus fibratus vertibratus" clouds (see Figure 6*a*).

In the limit case where the symmetric part of G has a zero eigenvalue ($d^2 = c^2 + f^2$; see Figure 4*b*), the ellipses "touch" along two (scale invariant) logarithmic spirals, each of which goes through an infinite number of rotations (but in opposite directions) as λ goes from $0 \rightarrow \infty$. Incidentally, log-spirals have played a prominent role in meteorological literature since at least *Guldberg and Mohn* [1877] (see also Figure 6*b*).

4. Generalized Scale Invariance Illustrated by the Fractal Sums of Pulses Process

4.1. *Modeling Vertical Rain and Cloud Cross Sections*

In this section we outline how linear scaling matrices of the form

$$\mathbf{G} = \begin{bmatrix} 1 & b & 0 \\ a & 1 & 0 \\ 0 & 0 & H_z \end{bmatrix}$$

can be used to model both differential stratification and rotation.

We have argued that the differential stratification of meteorological fields may be accounted for in the context of GSI by assuming that the ratio of horizontal and vertical scaling exponents (H_h/H_v) is $\frac{5}{9}$ and hence that the effective dimension of space is $D_{el} = 2 + \frac{5}{9} = 2.5555\ldots$, instead of 3.

By ignoring for the moment the rotation in the horizontal (studied in the next section) we can investigate the stratification effect along the vertical with $\mathbf{G} = (^{1}_{0}\ ^{0}_{H_z})$ (i.e., $D_{el} = 1.5555$ with $H_z = \frac{5}{9}$). Note this is equivalent to studying the vertical structure after averaging along the different horizontal directions.

The simplest way of implementing the FSP process in a space with an elliptical metric is to associate the pulses with the balls (B_λ) defined by the metric. Starting with an initial pulse base (B_1, e.g., a circle) at $\lambda = 1$, the pulse bases at larger and smaller scales are obtained by the equation $B_\lambda = T_\lambda B_1$.

The implementation of the FSP process with GSI therefore requires knowledge of (1) the operator T_λ (here we take

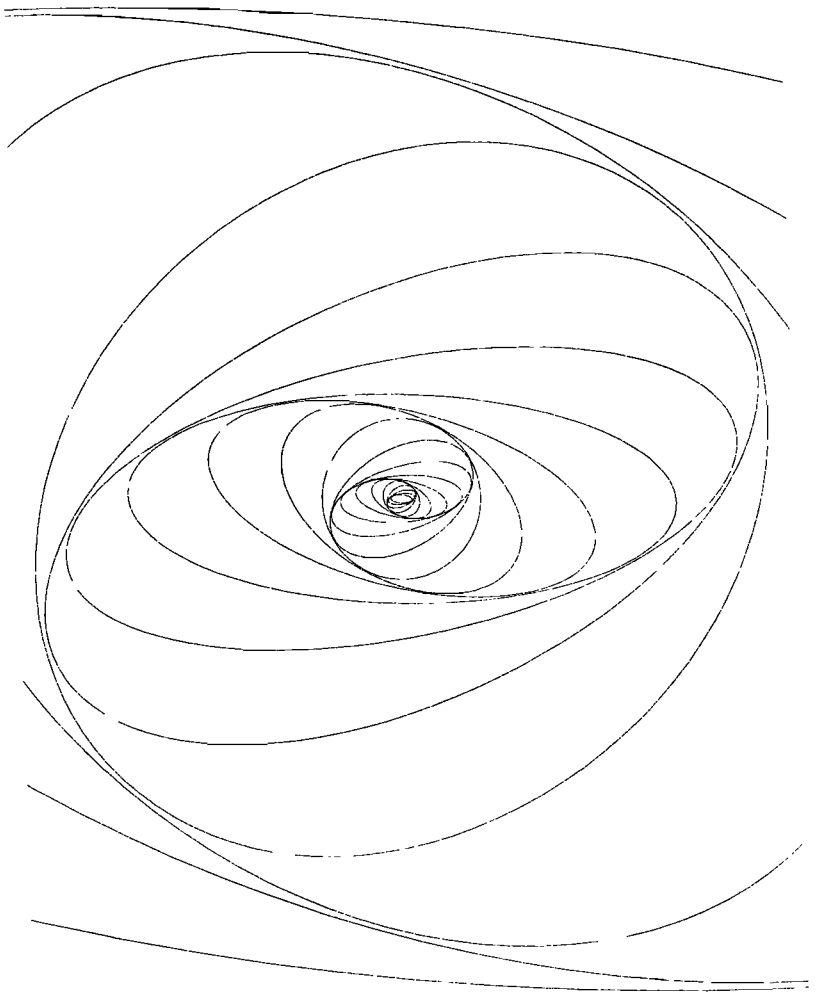

Fig. 4*b*. Same as Figure 1 except for $\mathbf{G} = \begin{pmatrix} 1 & -1 \\ 3 & 1 \end{pmatrix}$, $a^2 = -3$, and the ellipses "touch" along a scale invariant spiral (the symmetric part of G has a zero eigenvalue: $d^2 = c^2 + f^2$).

$T_\lambda = \lambda^{\mathbf{G}}$, $\mathbf{G} = \begin{pmatrix} 1 & 0 \\ 0 & 5/9 \end{pmatrix}$ and (2) the "pulse base" B_1. When $D_{el} < E$ (the euclidan dimension of space), a convenient way of defining B_1 exists. At very small scales, the horizontal fluctuations are greater than the vertical fluctuations. However, as the scale is increased, the amplitude of the vertical fluctuations grows rapidly (because $H_v > H_h$), and at some scale (called the "spheroscale" in the works by *Schertzer and Lovejoy* [1985*a*, *b*, also unpublished manuscript, 1983], the two have the same amplitude. On physical grounds we expect that the exact value of this distance may vary considerably, since it will depend on the relative intensities of the energy transfer (which determines the horizontal amplitudes) and the buoyancy force (which determines the vertical amplitudes). A proper treatment of this variability (which implies that the metric varies from place to place) requires the use of the nonlinear scaling described in the work by *Schertzer and Lovejoy* [1985*a*]. The shape of the average eddy at this scale may be used to define the ball B_1. In the work by *Schertzer and Lovejoy* [1985*a*] this scale was called the spheroscale because it was assumed that B_1 would be the simplest possible shape (a sphere). On purely mathematical grounds, the ball at the spheroscale is not necessarily a sphere. However, we shall continue to use this expression since it is the simplest and most physically appealing choice (unless it can be shown to be incompatible with some supplementary physical requirements).

Figure 7 shows the effect of varying the spheroscale from 1 pixel through 10,100,1000 pixels on a 400 × 400 point grid.

The shape at $\lambda = 1$ was a circle (these distances therefore correspond to isotropy) and the sequence may be regarded as a zoom by factors of 10 showing random vertical cross-sections at progressively higher resolution. At first, the field is very horizontally stratified reminiscent of stratus cloud decks (Figure 7, top left; spheroscale = 1 pixel); as the spheroscale is increased, we first notice the appearance of small "dangling" structures perpendicular to the overall stratification (Figure 7, top right; spheroscale = 10 pixels). When the spheroscale = 100 pixels (Figure 7, bottom left) it is comparable in size to that of our entire field of view. The very large scale horizontal stratification is still visible, but it is not very pronounced, and vertically oriented "streaks" are quite noticeable. Finally, at very high resolution (Figure 7, bottom right; spheroscale = 1000 pixels) the horizontal stratification disappears from view, and the streaks take on the appearance of vertically aligned rain shafts or intense cores.

Although this model is by no means perfect, it is encouraging that such realistic results can be obtained from such a simple process. Recall that the basic elements are (1) the

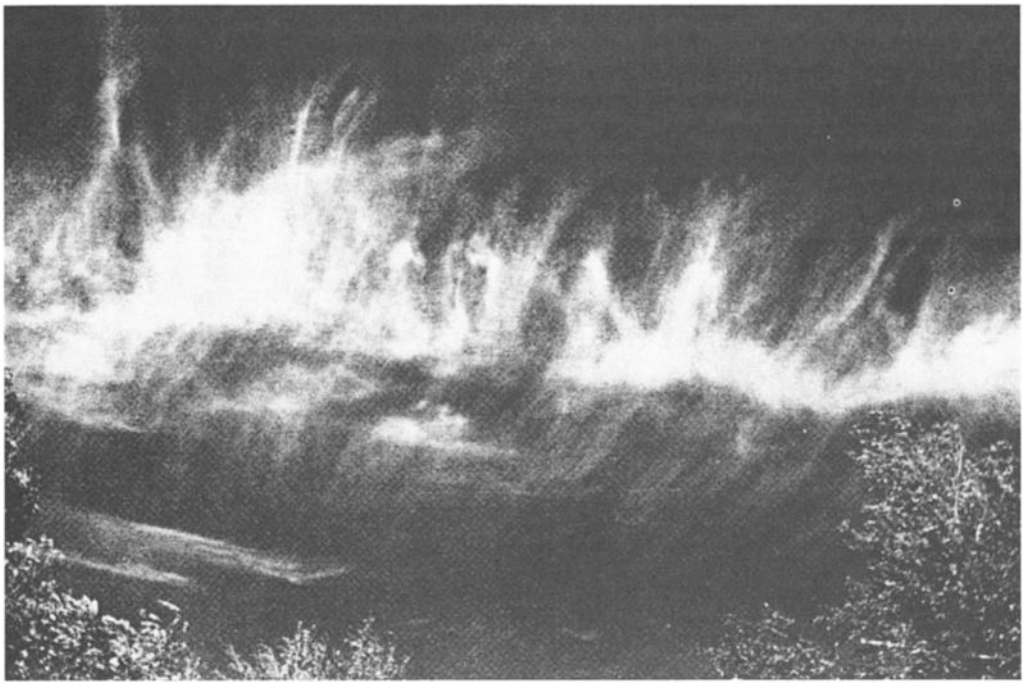

Fig. 5. Meteosat IR cloud photograph over north Africa showing a 3000-km-long east-west band composed of small-scale (~10 km wide) "fibers" aligned nearly north to south.

extreme intermittency (characterized by $\alpha \sim \frac{5}{3}$) and the differential stratification characterized by $D_{el} = \frac{23}{9}$. Much further study is required to determine the exact scaling and intermittency parameters and to suggest more realistic models (see, however, sections 5 and 6). It is also necessary to confirm that D_{el} is the same in the rain and wind field. As a final example of vertical stratification, see Figure 8 with a nondiagonal **G**. As expected, the diagonal elements yield a large-scale stratification, although at a somewhat oblique angle.

4.2. *Modeling the Effects of the Coriolis Force: Differential Rotation*

It is well known that atmospheric structures become increasingly "zonal" (i.e., east to west) at larger scales. At the same time, there is no obvious reason to expect atmospheric fields to scale differently (e.g., to have different values of β) in the north to south as compared to the east-west direction. For example, in the wind field, we expect energy transfer from large to small scales to be the dominant process determining the scaling of horizontal wind fluctua-

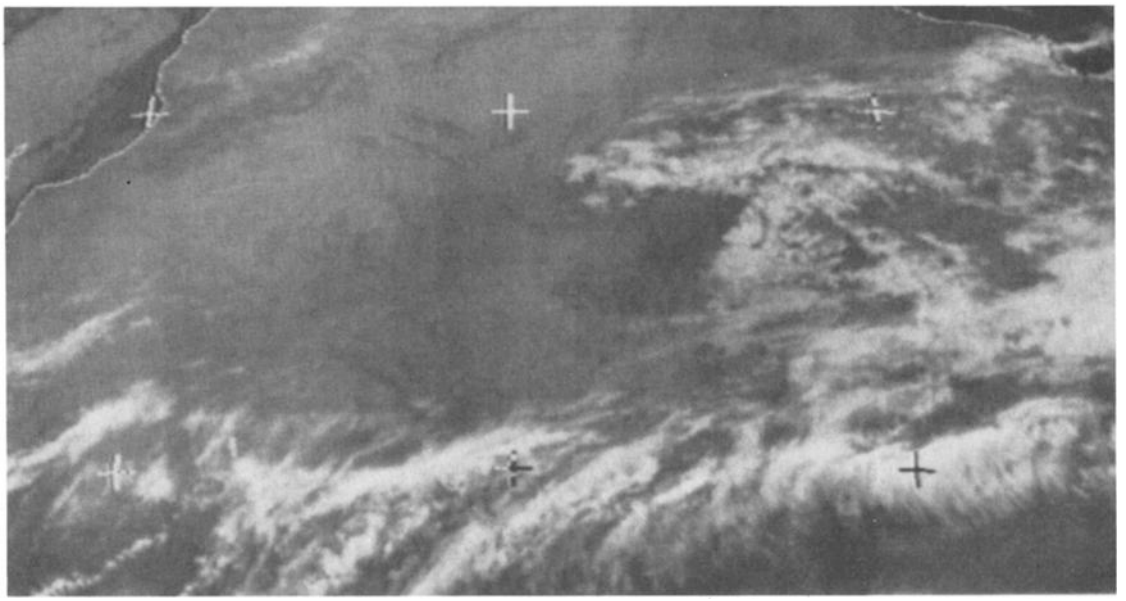

Fig. 6*a*. Cirrus fibratus vertibratus reproduced from plate 115 of the World Meteorological Organization international cloud atlas (volume 2). The scale is ~1000 times smaller than in Figure 5, and again, clearly shows perpendicular large- and small-scale structures.

Fig. 6*b*. Satellite picture of a mid-latitude cyclone; compare with the spiral in Figure 4*b*.

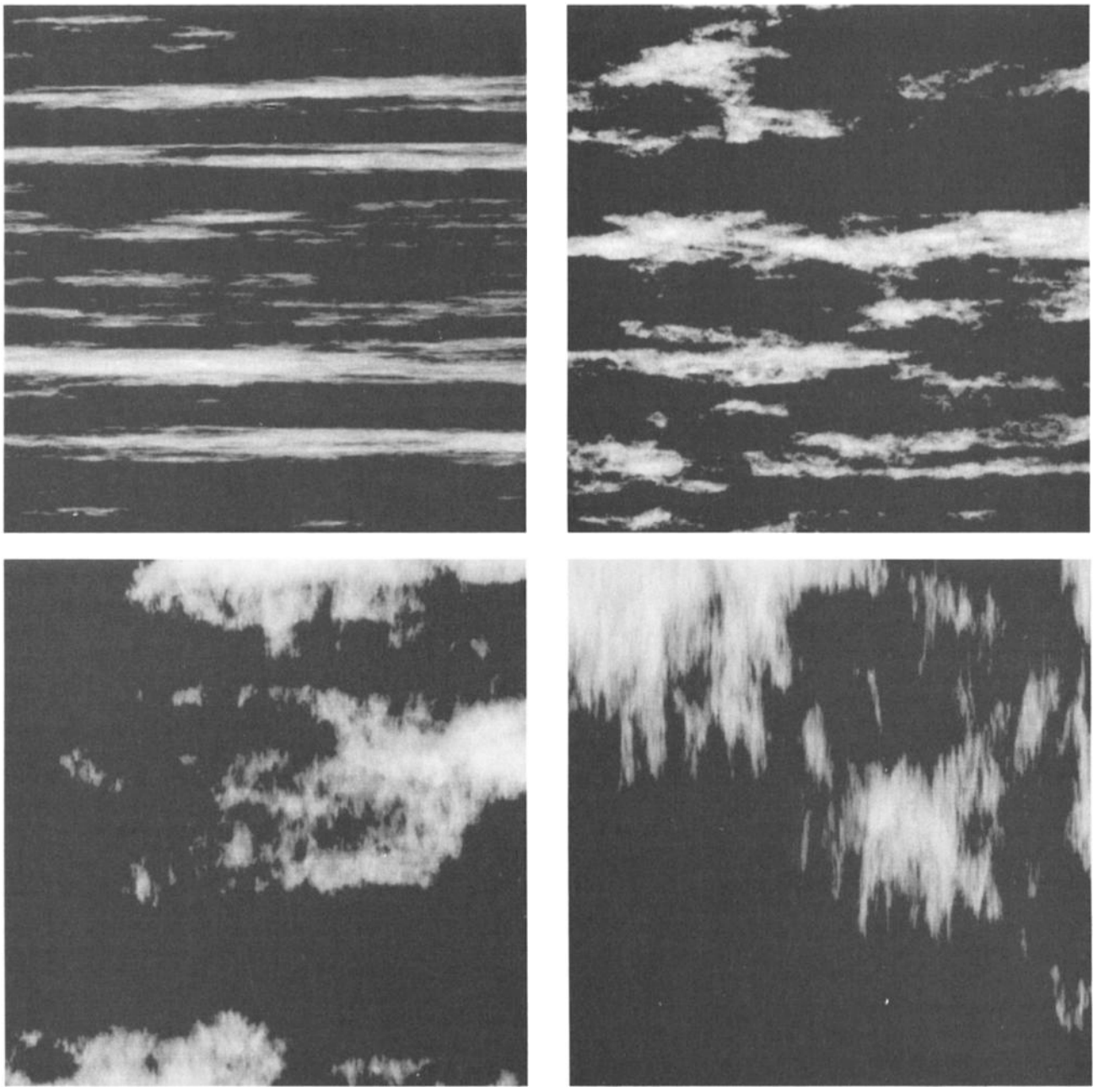

Fig. 7. Examples of random cross sections of an FSP process on a 400 × 400 grid with rain intensities as in Figure 2, with an anisotropic metric, $\mathbf{G} = \begin{pmatrix} 1 & 0 \\ 5/9 & \end{pmatrix}$ (hence $D_{el} = 1.5555$). See text for discussion.

tions in both north-south and east-west directions. This idea is well confirmed by studies of wind spectra: one obtains approximately $H_h = \frac{1}{3}$ along both horizontal axes. Recently obtained spectra analyzed in the work by *Lilly and Petersen* [1983] show a difference which is so small that it is probably not statistically significant. In the case where the north-south and east-west scaling exponents are identical we have $D_{el} = 2$ for the elliptical dimension of horizontal cross sections. The matrix **G** associated with the horizontal metric must therefore have the form $\mathbf{G} = \begin{pmatrix} 1 & \\ b & \end{pmatrix}$ (hence $d = 1$ and $c = 0$). The differential rotation is determined by the values of a, b.

In this case, the ratio of the north-south and east-west fluctuation amplitudes is constant, and the only convenient way to select B_1 is as a horizontal section of the ball at the spheroscale discussed earlier. Note that B_1 and the values of a,b are latitude dependent, since the Coriolis force varies with latitude. The use of fixed values of a,b (linear GSI) thus corresponds to the "f plane" approximation.

Figure 9 shows a series of FSP simulation with different values of a,b. For simplicity, B_1 was arbitrarily chosen to be a circle at the spheroscale. Note the perpendicularity between the largest and smallest scales (particularly in Figure 9, top left) which may be compared to the real cloud pictures shown in Figures 5 and 6*a*. The resemblance of these FSP simulations and real clouds is striking especially considering that no effort has been made to take into account the multiple scattering processes which determine the appearance of real clouds. It is possible, that at least to first order, the light scattered by clouds depends on the logarithm of the total water substance

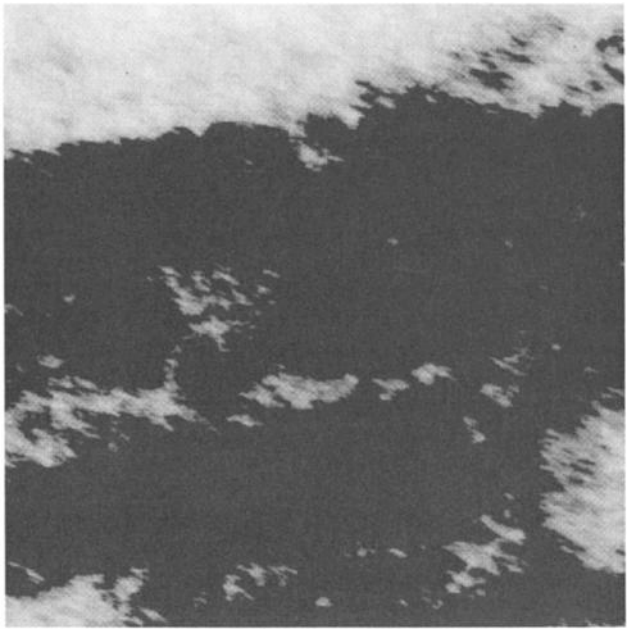

Fig. 8. Similar to Figure 7 with spheroscale = 100 units and D_{el} = 1.555, but here, there is some rotation.

(the optical depth), which is closely related to the rain rate integrated along a given direction.

5. Scaling Clusters of Pulses Process

The FSP process models the rain field by superposing a large number of basic shapes (the pulses). The fact that the resulting process has many of the same statistical properties as the real rain field poses the question as to whether the pulses have a physical counterpart or if they are simple mathematical artifacts. This question is real because unlike the case of Gaussian fluctuations where the shapes of the pulses would not matter, here, the biggest pulses are strong enough to dominate the sum of the others (the "Noah effect"), and thus the pulse shape is important. Since atmospheric eddies are likely to be complicated, twisted vortex tubes, the limitation to rather artificially simple pulse shapes (such as the circles and ellipses used in sections 2 and 4) is unfortunate.

Another problem with the FSP process used in sections 2 and 4 is that $H = 1/\alpha$, whereas radar data suggests $H \sim 0.50$ and $1/\alpha \sim 0.60$. B. Mandelbrot (unpublished manuscript, 1985) suggests a way of allowing $H < 1/\alpha$ by modifying the relationship between ρ and R. We do not follow this approach but suggest an alternative which allows for a physically appealing interpretation of the basic pulse shape.

Consider pulse intensities (ΔR) and durations (ρ) as before, in a space of euclidian dimension E. Rather than distributing the pulse centers uniformly over this space as was done in the FSP process, distribute them over a set of points with fractal dimension $D < E$. Such a set of points forms clusters at all scales (see for example, Figure 9). If the basic pulses are the same as those used previously, then the field resulting from all pulses associated with a given cluster of pulse centers, rather than individual pulses, may be considered as the basic model shape. By judicious choice of the distribution of pulse durations (see below), each of these clusters can be made to be scaling (a fractal) and the sum of all the clusters to itself be scaling. The cluster of pulses might plausibly correspond to a true eddy in the rain field.

We now show that the distribution of pulse durations may be chosen to ensure that the overall process is scaling.

Consider the one-dimensional SCP process. Denote by $n(L)$ the number of pulse centers within a distance L of a randomly chosen point on the line. If these centers form a set of dimension D (<1), then $n(L) \propto L^D$. Next, choose pulse durations (sizes) such that $Pr(\rho' > \rho) \propto \rho^{-\zeta}$ and intensities such that $\Delta R = \pm \rho^{1/\gamma}$. Now, change scales by the factor λ: $L \rightarrow \lambda L$, $\rho \rightarrow \lambda\rho$. The process is scale invariant if the number of pulses exceeding size ρ in a region of size ($= n(L)Pr(\rho' > \rho) = L^D\rho^{-\zeta}$) is invariant under this transformation. We therefore require $D = \zeta$. This scale transformation changes the amplitudes by $\lambda^{1/\gamma}$: $\Delta R \rightarrow \lambda^{1/\gamma}\Delta R$. The scaling parameter H therefore $= 1/\gamma$. The amplitudes are distributed as $Pr(\Delta R > \Delta r) \propto \Delta r^{-\gamma\zeta}$. Thus our intermittency exponent is given by $\alpha = \gamma\zeta = D/H$ or $D = \alpha H$. If we generalize our simulation to the plane, then the corresponding formulae are $Pr(A > a) \propto a^{-\zeta/2}$, $n(L) \propto L^D$, $R = {}^{+}_{-} A^{1/\gamma}$, and we obtain $D = 2\alpha H$. Similarly, for simulations in a space with dimension D_{el}, we obtain $D = D_{el} \propto H$. Note that for the FSP process, $D = D_{el}$, and the formulae reduce to the familiar $\alpha = 1/H$.

If we consider the horizontal rainfield, we have $D_{el} \sim 2$, $\alpha \sim \frac{5}{3}$, $H \sim \frac{1}{2}$; thus we require $D \sim \frac{5}{3}$. Therefore if the pulse centers are distributed on a set of dimension $D \sim \frac{5}{3}$, (e.g., Figure 10) and the pulse areas are distributed as $Pr(A > a) \propto a^{-5/6}$, then we may obtain a process with parameters $\alpha = \frac{5}{3}$ and $H = \frac{1}{2}$.

In practice, there are many ways of producing a set of points with dimension D. *Mandelbrot* [1982] calls sets with topological dimension zero "dusts"). When $D < 2$, the simplest is to use a "Levy Flight." One starts at the origin and chooses a randomly oriented vector with length (L) distributed according to $Pr(L > L) \propto 1^{-D}$. The tip of this vector marks the second point of the set: the process is repeated from the new starting point until a sufficient number of pulse centers have been generated. If this process is repeated for an infinity of points and the length of each vector is diminished to zero, the resulting set has dimension D. This process produces scaling clusters of points because the distribution L^{-D} occasionally produces enormous jumps (the "Noah effect" again). However, any other construction mechanism (e.g., *Mandelbrot*'s [1982] trema construction for the distribution of galaxies) will generate clusters at all scales; clustering is an intrinsic property of such sets. These other construction mechanisms will differ from the Levy flight in that their lacunarity may be quite different. Indeed, the set shown in Figure 10 probably has too many large, vacant lacunar regions: a less inhomogeneous SCP process should result if a less lacunar construction mechanism is used.

Figure 11 shows an example of the SCP process on a 400 × 400 point grid. Two key differences with the FSP process may be noted. First, the pulses associated with one particular cluster of centers stands out: it is roughly circular at the spheroscale, with a long band trailing away from it. The G matrix was chosen so that rotation would predominate; the clustering of centers gives us a definate feeling of rotation which was absent in the FSP process, since there, pulses with different orientations were superposed uniformly, and only the extreme (large- and small-scale orientations) stood

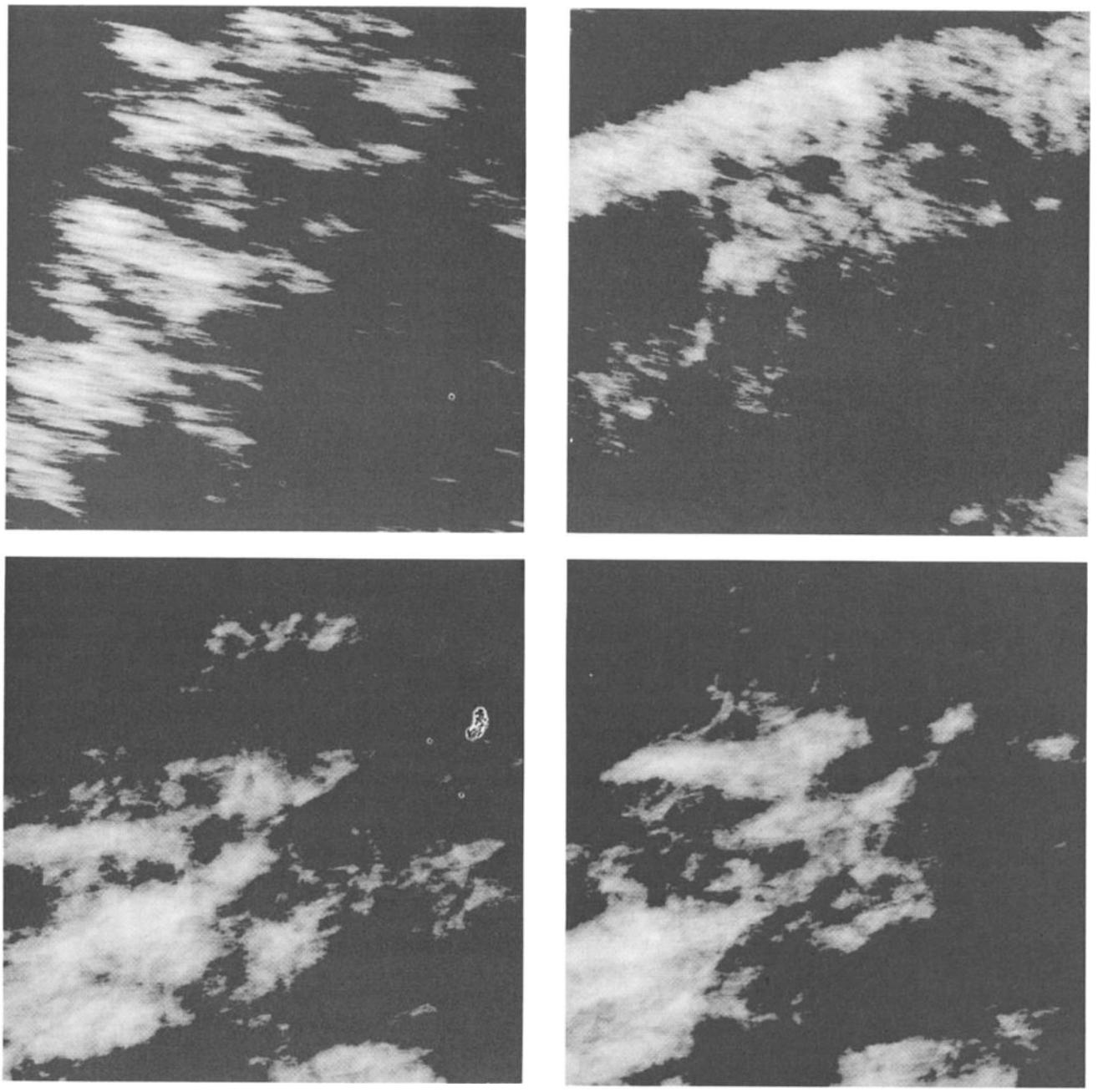

Fig. 9. Examples of FSP processes on 400 × 400 grids modeling the effect of the Coriolis force with $H_z = 1$ for varying degrees of rotation and stratification. (*a*) Spheroscale = 400; (*b*) spheroscale = 100; (*c*) spheroscale = 50; (*d*) spheroscale = 1200 pixels.

out. The SCP process can therefore produce a crude model of the clouds associated with mid-latitude cyclones.

The second key difference with the FSP process is the high degree of nonuniformity resulting from the clustering: some regions have fairly smooth shapes, while others are extremely complicated. At first sight it would seem that the dimension of the perimeters (D_p) has been reduced in comparison with the FSP process. Actually, the opposite is the case; as we show in the next section, the dimension of the perimeter is $\frac{3}{2} = 1.5$ (compared to $\frac{7}{5} = 1.4$ for the simulations in sections 2 and 4). This increase occurs because over small regions, the perimeter is extremely complex; in the formula $P \propto \sqrt{A}^D P$ we could say that most of the "length" of P comes from very small regions of A, the rest being relatively smooth. This variation of smoothness corresponds to our intuitive feeling about real cloud and rain areas.

At the same time, as the clustering of centers tends to produce regions of high complexity, it tends to break up cloud or rain areas into many smaller ones; in other words, the exponent B in the rain area distribution increases (there are more small areas compared to large ones). This visual impression is correct: numerical simulations yield $B \sim 0.75 \pm 0.05$ for the SCP process (with $\alpha = \frac{5}{3}$ and $H = \frac{1}{2}$), while the corresponding value for FSP (with $\alpha = \frac{5}{3}$ and $H = \frac{3}{5}$) is $B \sim 0.5 \pm 0.05$ [*Lovejoy and Mandelbrot*, 1985]. Since the empirical value is $B \sim 0.75$, the SCP process is in this respect statistically more realistic than the FSP process. It is possible that variations on the SCP theme (many of which we

Fig. 10. Example of a Levy flight with $D = \frac{5}{4}$, with 20,000 points. See text for details.

tried and abandoned) could yield even more realistic cloud and rain simulations. However, in the next sections we argue that both FSP and SCP suffer from what may be a fundamental limitation: they are characterized by a single dimension. Probably much more experimental and theoretical work is needed before more complicated models should be used.

Table 1 shows a comparison of the data with the FSP and SCP processes. The latter yields a better fit for all the fractal parameters except the dimension of the perimeters.

6. Numerical Renormalization Method for Calculating Fractal Dimensions in FSP and SCP Processes

6.1. *Zero-Crossings and Perimeters*

From the preceding discussion it is clear that the selection of a realistic rain model depends at least partly on an accurate determination of the fractal parameters D_p, D_{el}, w, H, B, etc from both the data and the models. Empirical determination of these parameters is, in general, difficult because the parameters depend on the logarithm of physical or model quantities: the latter must therefore span many orders of magnitude in scale.

It is thus of considerable importance that as many model parameters as possible be determined theoretically. In particular, we would like to answer the following two questions: first, what is the dimension of model perimeters, and second, does the dimension depend on the threshold R_T or is it constant? In other words, are the very intense regions of the model concentrated in a set with a smaller fractal dimension than the less intense regions? (Is the field multidimensional?).

The rain area perimeters defined in the FSP and SCP process are the curves defined by $R(x, y) = \text{const}$ (with dimension D_P, which we temporarily denote D_{P2}). If the process is isotropic in x, y the dimension of $R(x, 0)$ (a one-dimensional section) has dimension $D_{P1} = D_{P2} - 1$ (this is the fractal analogy of the usual geometric theorem on the dimension of intersections of lines, planes etc.). It is therefore only necessary to determine D_{P1}. In the case of fractional brownian motion (the increments of this process are gaussian), the formula $H + D_P = 2$ is known to hold (or $H + D_{P1} = 1$), and *Hentschel and Procaccia* [1984] use this formula to theoretically calculate D_P from H (they obtain $D_P = 1.38$ for passive scalar clouds). Although there is reason to suspect this formula to be valid for many processes, it is clearly not valid for all: *Mandelbrot*'s [1974] cascade model (see next section) is stationary and can be adjusted to allow the value of D_P to vary (there, D_P also depends on the threshold; it is multidimensional) (see, for example, *Mandelbrot* [1984] and *Schertzer and Lovejoy* [1985*b*]. Furthermore, the data for rain suggests $H + D_P \sim 0.50 + 1.35 = 1.85$. It is therefore of interest to be able to determine D_P by numerical simulation. The calculation described in the following subsection confirms $H + D_P = 2$ for both the FSP and SCP processes.

6.2. *Numerical Renormalization Method*

Chorin [1982] describes a numerical renormalization method that can be used to accurately determine the dimension of the zero-crossings of Brownian motion. His method is very specialized: it depends on the existence of interpolation formulae for Brownian motion. In essence, rather than estimating the dimension from the number of zero-crossings of an enormous sample function $R(t)$, only values of $R(t)$ near zero-crossings are calculated. By zooming in on areas of $R(t)$ near the t axis, Chorin was able to stimulate a Brownian motion function 10^{400} pixels long, obtaining estimates of D_{p1} within 0.1% of the theoretical value ($= \frac{1}{2}$).

In order to generalize Chorin's method so as to apply it to FSP and SCP processes, we calculated a sample function over a fairly short length (L typically 500 pixels long). Pulses were taken to be rectangularly shaped, and all pulses between the outer scale L and 1 grid length were added (this is the minimum resolution). Next, all sections such that $|R(t)| > \sigma$, where σ is a threshold, were deleted, resulting in a number of short segments (representing a fraction f of the total length L) within a distance σ of the t axis. If σ is taken to be sufficiently large, then there is a very small chance that bellow grid scale fluctuations in $R(t)$ would have produced one or more zero-crossings on the deleted sections and the sections retained therefore contain virtually all the zeroes in the segment (in practice, $\sigma = 3$ yielded satisfactory results; this corresponds to three times the largest fluctuation likely to occur at subgrid scales).

The next step in the process is the "zoom" or renormalization in which we attempt to discern the number of subresolution zero-crossings. We enlarge the collection of segments

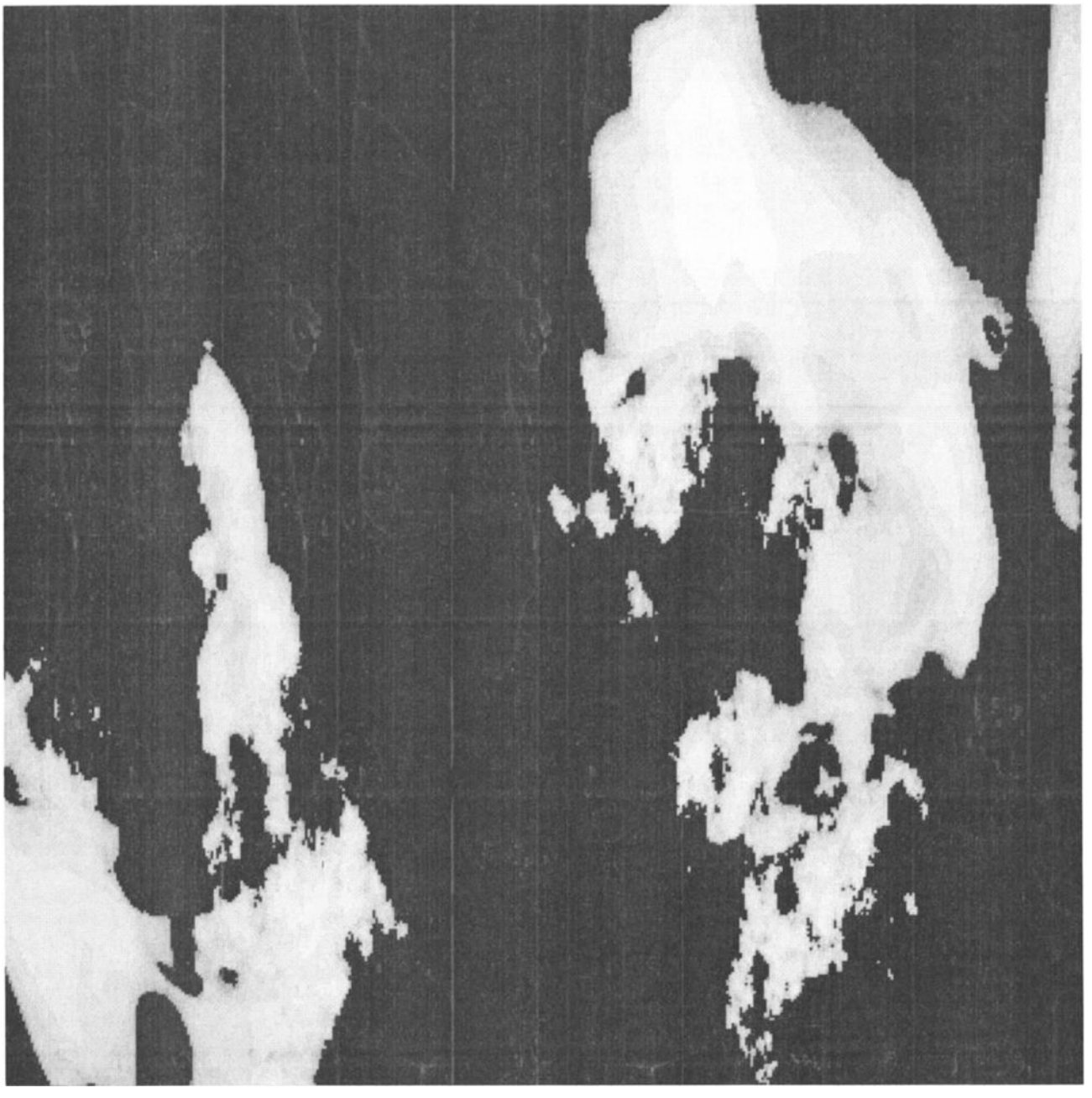

Fig. 11. Example of an SCP process on a 400 × 400 grid, with $\alpha = \frac{5}{3}$ and $H = \frac{1}{2}$ (and $\Lambda = 1.1$); the spheroscale is 100 pixels. The differential rotation, coupled with the clustering of echo centers, yields a crude model of a mid-latitude cyclone (see the structure concentrated in the upper right-hand corner). Note the highly nonuniform perimeters (dimension = 1.5).

(of total length Lf, $f < 1$) by the factor $\frac{1}{f}$ so that they fit exactly into the array $R(t)$ which now contains the enlarged segments. Finally, the renormalization process is completed by multiplying the $R(t)$ values by $(1/f)^H$ and then adding in small-scale random fluctuations between the old enlarged inner scale $\frac{1}{f}$ and the new inner scale = 1.

The new series contains virtually all the zero-crossings that would have occurred in a function of length $\frac{L}{f}$. In practice, $f \sim 0.6 - 0.2$ so that each "renormalization" gains a factor of $\sim 1.5 - 5$ in effective length. If we repeat the process several times, eventually we obtain a number of zeroes (N) comparable to the number of grid points used (e.g., $N \sim 0.2L$). Empirically, saturation with zeroes actually occurs when $N \sim 0.2L$ because each segment must be at least three elements long : two end points and a center with one or two zero-crossings.

With $L = 500$ and $H = \frac{1}{\alpha} = \frac{3}{5}$, saturation occurred when the effective length was about 10^7 (yielding $D_{p1} = 0.38 \pm 0.08$), so that even without going further we have achieved a gain in effective length of factor $\sim 10^4$ (when $H = \frac{1}{\alpha} = \frac{4}{5}$ we obtained $D_{p1} \sim 0.17^+ - 0.07$ with an effective length of 10^{13}: the gain is larger because the set of zero-crossings is sparser). In order to exceed these limits, we must "prune" the segments further. This can be accomplished by eliminating at random half of the $R(t)$ function and renormalizing the remaining half by the factor 2. On average, this process

TABLE 1. Various Fractal Parameters Estimated From Both the Data and FSP and SCP Simulations

		H_E	B	D_p
Data	1.66 ± 0.05*	0.50 ± 0.02†	0.75 ± 0.05‡	1.35§
FSP	$\frac{5}{3}$	$\frac{3}{5}$	0.50 ± 0.05	7/5‖
SCP	$\frac{5}{3}$	$\frac{1}{2}$	0.75 ± 0.05	3/2‖

* Data for GATE, Montreal, and for Spain.

† GATE data yield 0.48 ± 0.02 and Montreal data yield 0.50 ± 0.05.

‡ GATE data only.

§ GATE and Indian Ocean data yield $D_p = 1.35$ [Lovejoy, 1982], data over France yield $D_p = 1.38$ [Lovejoy et al., 1983], and data over the Mediterranean yield $D_p = 1.345$ (R. Cahalan et al., unpublished manuscript, 1984). Note that these dimensions are for warm, low clouds, and low rain rates-intense regions may be expected to have smaller values.

‖ These values are obtained by using the formula $H + D_p = 2$.

eliminates half the zero-crossings, so we obtain an "effective" N_{eff} which is twice the previous value.

In practice, a threshold $f_T \sim 0.15$ set, so that "pruning" occurs each time $N > Lf_T$. The entire process of renormalization and pruning is repeated until L_{eff} and N_{eff} are sufficiently large (typically 150 iterations yield $L_{eff} \sim 10^{32}$ and $N_{eff} 10^{13}$ for $H = \frac{1}{\alpha} = \frac{3}{5}$). D_{p1} is estimated by a regression of log L_{eff} versus log N_{eff}. The table below shows the result of several runs on a CDC 175 computer, each requiring ~30 s of CPU time. The determination of D_{p1} for $H = \frac{1}{\alpha} = \frac{3}{5}$ with $\sigma = 3$, each run consisting of 150 iterations, is given below. The effective sample length (L_{eff}) was $\sim 10^{32}$, and the effective number of zeroes (N_{eff} was $\sim 10^{13}$). This yields an estimate of $D_p = 1.3993$ for perimeters of the two dimensional process (thus $H + D_p = 1.993$). The average value of D_{p1} equals 0.3993 ± 0.0251.

0.3874	0.4026	0.4081
0.3589	0.4351	0.4036

The results of this renormalization scheme clearly support the use of the formula $H + D_p = 2$ for both FSP and SCP processes. Note, however, that the clustering of pulses in the SCP process leads to a much wider dispersion in the estimates of D_{p1} in that case. They also show that D_p, and D_{p1} are independent of the threshold (i.e., the value of D_{p1} for the set of zero-crossings of the line $R(t) = R_T$ is independent of R_T). FSP and SCP processes are therefore monodimensional.

Note that this method does not lend itself easily to the calculation of the area distribution exponent B. In particular, the formula $B = D_p/2$ applicable to Gaussian processes [see *Mandelbrot*, 1982] seems to be definitely ruled out by the numerical calculations performed in the work by *Lovejoy and Mandelbrot* [1985].

7. Beyond FSP and SCP: Some Elements of Multidimensionality

A fractal set or measure which is not "homogeneous" in the sense of *Hentschel and Procaccia* [1983] has multiple fractal dimensions. The possibility of such nonhomogeneity was first raised by *Hentschel and Procaccia* [1983] and *Grassberger* [1983] in the context of strange attractors. These authors observed that in strange attractors, two-point correlation functions (which depend on the clustering of point pairs) do not in general scale in the same manner (they have a lower dimension, D_2) as compared to the overall density of points (D or as, in general, the analagous n point correlation functions which have dimension, D_n). As one goes to smaller and smaller scales, the structure of the set is increasingly dominated by dense clumps of points which are themselves increasingly sparsely distributed (eventually one reaches a minimum D_∞).

At about the same time, and independently [*Mandelbrot*, 1984; *Schertzer and Lovejoy*, 1985*b*; D. Schertzer and S. Lovejoy, unpublished manuscript, 1983] it was shown that a process first introduced by *Mandelbrot* [1974] to study cascade processes yields a measure characterized by an infinite hierarchy of dimensions of support. *Parisi and Frisch* [1985] have coined the term "multifractals" for a model of possible solutions of the Navier-Stokes equations based on essentially the same ingredients but presented in different terms. They also showed how the multiple fractal dimensions in turbulence could be measured from high-order structure functions.

It now seems that multidimensionality is quite natural: a priori, it would seem to be much more so than the homogeneous monodimensional case. In particular, *Schertzer and Lovejoy* [1985*a*, *b*, also unpublished manuscript, 1983] showed that in curdling, divergence of high moments and multidimensionality occurs in every case, except in the trivial "β model" [*Frisch et al.*, 1978]. The realization that multidimensionality may be the rule rather than the exception suggests on the one hand that the data should be reanalyzed more carefully (e.g., the range of thresholds used to define cloud and rain areas in *Lovejoy* [1982] should be greatly extended, especially to isolate small active regions) and on the other hand, that realistic multidimensional rain models should be developed.

For the purposes of rain modeling, *Mandelbrot*'s [1974] cascade model suffers from two weaknesses. First, the process itself rather than its increments is stationary, and second, it suffers from strong dependence on an initial grid which makes simulations look quite artificial. This paper is not the place for a detailed exploration of these and related issues. Undoubtedly, both these problems are soluable (for instance, more general scaling measures than the one resulting from Mandelbrot's cascade model are indicated in the work by *Schertzer and Lovejoy* [1985*b*], and will be the subject of considerable development in the near future.

8. Conclusions

In this paper we have tried to synthesize and develop previous work on scaling and intermittency in the atmosphere. We have argued that while the atmosphere cannot be self-similar (the small scales a carbon copy of the large), that it does obey a related symmetry principle called generalized scale invariance in which the relationship between small- and large-scale structures involves not only magnification but also differential rotation and stratification. On the other hand, the richness of atmospheric structures and the phenomenology of sudden changes (intermittency) require that fluctuations be very strong; specifically, be hyperbolic in form.

These ideas were illustrated with various models of the

rain and cloud fields. The first model studied, the fractal sums of pulses process, models the rain field by a hierarchy of simple "pulse" shapes. In a second model (the scaling cluster of pulses process) the pulse centers are clustered so that the basic element maybe regarded as a complex (fractal) pulse. This model gave closer agreement with the measured fractal parameters of rain. The FSP process was used to illustrate both the horizontal stratification of rain and the differential rotation associated with the Coriolis force. In spite of its simplicity, simulations were visually realistic; for example, they could display the perpendicularity of the large- and small-scale structures visible in many real cloud photographs. The SCP process was apparently more realistic: it was possible to use it as a crude model of mid-latitude cyclones, and the simulated shapes were far less homogenous than in the FSP process.

These models may prove to be useful in hydrology and elsewhere, since they capture the extreme variability and anisotropy of rain over a very wide range of scales in a very simple way. They have the further advantage of depending on clear physical principles.

A numerical procedure was described which enable fractal dimensions to be accurately calculated. A final section discussed the question of multidimensionality and pointed toward future developments.

Acknowledgments. We especially benefitted from discussion with B. Mandelbrot, R. Peschanski, and J. Peyrière. We also acknowledge G. Austin, P. Bougeault, R. Cahalan, V. Gupta, G. Hentschel, E. Hopfinger, I. Procaccia, M. Rafy, G. Therry and E. Waymire. One of us (S.L.) would like to thank B. Mandelbrot and the T. Watson research center, IBM for hospitality during the production of most of the simulations shown in this paper. This work was partially supported by the Centre Nationale de Recherches Scientifiques (ATP-RA (84) 16).

REFERENCES

Bhattacharya, N. N., V. K. Gupta, and E. Waymire, The Hurst effect under trends, *J. Appl. Probab., 20*, 649–662, 1983.

Bogliano, R., Turbulent spectra in a stably stratified atmosphere, *J. Geophys. Res., 64*, 2226–2230, 1959.

Brown, P. S., and G. D. Robinson, The variance spectrum of tropospheric winds over Eastern Europe, *J. Atmos. Sci., 36*, 270–286, 1979.

Chorin, A. A., Numerical estimates of Hausdorff dimension, *J. Comp. Phys., 46*, 390–396, 1982.

Frisch, U., P. L. Sulem, and M. Nelkin, A simple dynamical model of intermittent fully-developed turbulence, *J. Fluid Mech., 87*, 719–724, 1978.

Grassberger, P., Generalised dimensions of strange attractors. *Phys. Lett. A, 97*, 227–230, 1983.

Guldgerg, C. M., and H. Mohn, Die Bewegung der Luft in austeigenden Wirbeln, *Wien Met. Zeits., 12*, 259–267, 1877.

Hentschel, H. G. E., and I. Procaccia, The infinite number of generalised dimensions of fractals and strange attractors, *Physica D, 8*, 435–444, 1983.

Hentschel, H. G. E., and I. Procaccia, Relative diffusion in turbulent media: The fractal dimension of clouds, *Phys. Rev., Ser. A, 29*, 1461–1470, 1984.

Kolmogorov, A. N., A refinement of previous hypotheses concerning the local structure of tubulence in a viscous incompressible fluid at high Reynolds number, *J. Fluid Mech., 13*, 82–85, 1962.

Lilly, D. K., Meso-scale variability of the atmosphere, in *Meso-scale Meteorology—Theories, Observations and Models*, edited by D. K. Lilly and T. Gal-Chen, pp. 13–24, D. Reidel, Hingham, Mass., 1983.

Lilly, D., and E. Petersen, Aircraft measurements of atmospheric kinetic energy spectra, *Tellus, 35*, 379–382, 1983.

Lovejoy, S., A statistical analysis of rain areas in terms of fractals, paper presented at 20th Radar Conference, Am. Meteorol. Soc., Boston, 1981.

Lovejoy, S., The area-perimeter relationship for rain and cloud areas, *Science, 216*, 185–187, 1982.

Lovejoy, S., The fractal geometry of cloud and rain zones with random simulations, *Houille Blanche, 516*, 431–436, 1983.

Lovejoy, S., and B. Mandelbrot, Fractal properties of rain and a fractal model, *Tellus*, in press, 1985.

Lovejoy, S., and D. Schertzer, Scale invariance, symmetries, fractals and stochastic simulations of atmospheric phenomena, AMS Bull., in press, 1985*a*.

Lovejoy, S., and D. Schertzer, Scale invariance in climatological temperatures and the local spectral plateau, *Ann. Geophysi.*, in press, 1985*b*.

Lovejoy, S., and D. Schertzer, Extreme variability scaling and fractals in remote sensing analysis and simulation, in *Digital Image Processing in Remote Sensing*, edited by P. J. Muller and T. Francis, in press, 1985*c*.

Lovejoy, S., J. Tardieu, and G. Monceau, Etude d'une situation frontale: Analyse météorologique et fractale, *La Météorologie, 4*, 111–118, 1983.

Mandelbrot, B., Statistical methodology for non-periodic cycles: From the covariance to R/S analysis, *Ann. Econ. Soc. Meas., 1*, 259–290, 1972.

Mandelbrot, B., Intermittent turbulance in self-similar cascades: Divergence of high moments and dimension of the carrier, *J. Fluid Mech., 62*, 331–352, 1974.

Mandelbrot, B., *The Fractal Geometry of Nature*, 461 pp., Freeman, San Francisco, Calif., 1982.

Mandelbrot, B., Fractals in physics: Squig clusters, diffussions, fractal measures and the unicity of fractal dimensionality, *J. Stat. Phys., 34*, 895–930, 1984.

Mandelbrot, B., and J. R. Wallis, Noah, Joseph and operational hydrology, *Water Resour. Res., 4*, 909–918, 1968.

Novikov, E. A., and R. Stewart, Intermittency of turbulence and spectrum of fluctuations of energy dissipation, *Izv. Akad. Nauk. SSSR Ser. Geofiz., 3*. 408–412, 1964.

Obukhov, A. N., Effect of Archimedean forces on the structure of the temperature field in a turbulent flow, *Dokl. Akad. Nauk. SSSR, 125*, 1246–1200, 1959.

Orszag, S. A., Statistical theories of turbulence, in *Fluid dynamics*, edited by R. Balian and J. L. Peube, Gordon and Breach, New York, 1973.

Parisi, O., and U. Frisch, A multifractal model of intermittency, in *Turbulance and Predictability in Geophysical Fluids Dynamics and Climate Dynamics*, edited by M. Ghil, R. Benzi, and G. Parisi, pp. 84–88, North-Holland, Amerstam, 1985.

Richardson, L. F., *Weather Prediction by Numerical Process*, Dover, New York, 1922.

Rodriguez-Iturbe, I., V. K. Gupta, and E. Waymire, Scale considerations in the modelling of temporal rainfall, *Water Resour. Res., 20*, 1611–1619, 1984.

Rose, H. A., and P. L. Sulem, Statistical theories of turbulence, *J. Phys., 39*, 441–460, 1978.

Schertzer, D., and S. Lovejoy, Les Fractales dans l'atmosphère, *Sci. Tech.*, 69–72, May, 1984*a*.

Schertzer, D., and S. Lovejoy, The dimension and atmospheric motions, in *Turbulence and Chaotic Phenomena*, edited by T. Tatsumi, pp. 505–512, North-Holland, Amsterdam, 1984*b*.

Schertzer, D., and S. Lovejoy, The dimension and intermittency of atmospheric dynamics, in *Turbulent Shear Flow 4*, edited by B. Launder, pp. 7–33, Springer, New York, 1985*a*.

Schertzer, D., and S. Lovejoy, Generalized scale invariance in turbulent phenomena, *PCH J.*, in press, 1985*b*.

Waymire, E., Scaling limits and self-similarity in precipitation fields, *Water Resour. Res.*, this issue.

Waymire, E., and V. K. Gupta, The mathematical structure of rainfall representations, 1, A review of stochastic rainfall models, *Water Resour. Res., 17*, 1261–1272, 1981*a*.

Waymire, E., and V. K. Gupta, The mathematical structure of rainfall representations, 2, A review of the theory of point processes, *Water Resour. Res., 17*, 1273–1286, 1981*b*.

Waymire, E., and V. K. Gupta, The mathematical structure of rainfall representations, 3, Some applications of the point process theory to rainfall processes, *Water Resour. Res., 17*, 1287–1294, 1981*c*.

Waymire, E., V. K. Gupta, I. Rodriguez-Iturbe, A spectral theory of rainfall intensity at the mesoscale, *Water Resour. Res.*, *26*, 1453–1465, 1984.

Yaglom, A. M., The influence of the fluctuations in energy dissipation on the shape of turbulent characteristics in the inertial interval, *Sov. Phys. Dokl.*, *2*, 26–30, 1966.

Zawadzki, I. I., Statistical properties of precipitation patterns, *J. Appl. Meteorol.*, *12*, 459–472, 1973.

S. Lovejoy and D. Schertzer, Physics Department, McGill University, 3600 University Street, Montreal, Quebec, Canada H3A 2T8.

(Received September 12, 1984;
revised March 25, 1985;
accepted March 29, 1985.)